Fujishiro *et al. Journal of Wood Science* (2022) 68:15
https://doi.org/10.1186/s10086-022-02016-7

Journal of Wood Science

ORIGINAL ARTICLE

Open Access

Flexural vibration properties of particle board using acrylic emulsion adhesives with differential glass transition temperature

Kaoru Fujishiro[1], Takuya Ito[2], Hiroko Sato[3], Ryosuke Masunari[3] and Masaaki Yamada[3*]

Abstract

Vibration characteristics of wood-based materials are essential parameters in considering the indoor environment of a building. This study investigates the effect of the physical properties of water-based adhesives on vibration characteristics of wood-based materials. Adhesive films and particle boards (PB) were prepared from acrylic emulsion adhesives (AE) with differential glass transition (T_g), and loss tangent of dynamic viscoelasticity (tanδ_D) and flexural vibration property (tanδ_F) were compared. The tanδ_D master curve and tanδ_F showed a similar tendency regarding frequency dependence. The apparent activation energy (ΔH) calculated from the shift factor of the master curve tends to be different depending on the T_g of AE and was especially high for AE with $T_g = 13$ °C along with blended AE. The dynamic Young's modulus (E_F) calculated from the flexural vibration tests showed higher values for AE at $T_g = 13$ °C, 41 °C, and 90 °C than that of urea–formaldehyde adhesive (UF).

Keywords: Acrylic emulsion adhesive, Glass transition temperature, Dynamic viscoelasticity, Time–temperature superposition, Master curve, Apparent activation energy, Shift factor, Particle board, Flexural vibration, Loss tangent

Introduction

Since the industrial revolution in the latter half of the eighteenth century, the world population, which was less than one billion, has increased rapidly and is forecast to reach 9.7 billion by 2050. Most of the increased population lives in urban areas [1], and living noise due to the increase in apartments is viewed as a problem [2, 3]. In Japan, nearly 2500 complaints of noise originating from home life and store operations were received in 2019; most of them were concentrated in large cities [4]. Therefore, the control of indoor noise in urban areas is an important issue worldwide.

In Japanese urban areas, wooden constructions are used for low-rise buildings, and reinforced concrete (RC) and steel-framed RC (SRC) structures are used for mid-high-rise buildings. Furthermore, the number of wooden mid-high-rise apartments has been gradually increasing due to the recent progress of cross-laminated timber (CLT). Among them, floor impact noise countermeasures during wooden apartment buildings are probably important regardless of the size of buildings. As wooden constructions have lower stiffness and mass than RC and SRC constructions, resulting in lower floor impact sound insulation performance [5–7]. In addition, it has been reported that this tendency does not change even when CLT is used [8, 9]. Accordingly, impact sound countermeasures are essential in wooden apartment buildings, such as dry double floors, suspended ceilings, and damping materials. Failure to do so makes it difficult to satisfy adaptation class 3 [10], which is defined as the standard floor impact sound insulation performance in daily life summarized by the Architectural Institute of Japan. However, improving the floor impact sound insulation performance typically increases the construction

*Correspondence: yamada.masaaki@shizuoka.ac.jp
[3] Faculty of Agriculture, Shizuoka University, 836, Ohya, Suruga-ku, Shizuoka 422-8529, Japan
Full list of author information is available at the end of the article

cost; therefore, a construction method with low cost and high performance is important.

Research adding vibration damping properties to wood-based materials has been made to solve such problems. First, the vibration damping properties of general wood-based materials have been evaluated by Wang et al. [11] and Guan et al. [12] using the cantilever method, such as logarithmic decrement. Ebihara [13] successfully increased the loss tangent (tanδ) of particle board (PB) by blending pellets of agricultural polyvinyl chloride sheet. Lee et al. [14–18] examined the detailed relationship between laminated wood and tanδ from the dynamic viscoelasticity viewpoint by changing the differential glass transition (T_g) of nonaqueous adhesives. They successfully developed an adhesive with high tanδ over a wide temperature range by introducing an interpenetrating polymer network into the adhesive. Sargianis et al. [19] maintained bending stiffness and improved tanδ by bonding plant fibers impregnated with a vinyl ester resin to lightweight wood. In this way, various studies have been conducted on imparting vibration damping properties to wood-based materials. However, they are mainly the changes in the physical properties of nonaqueous adhesives and the addition of the resin pellets. A limited number of studies have investigated the relationship between changes in the physical and vibration damping properties of water-based adhesives, which are widely used in the production of wood-based materials.

Most water-based adhesives recently used in producing wood-based materials are formaldehyde-based adhesives using urea resin, melamine resin, and phenol resin. However, we hope that these shift to non-formaldehyde adhesives such as aqueous emulsions because they contain formaldehyde of hazardous substance. One of the non-formaldehyde adhesives is a thermoplastic acrylic emulsion adhesive (AE). AE is made from emulsion polymerization of acrylic acid and methacrylic acid esters. AE characteristics are abundant in many monomers compared with other resins; they can be copolymerized or otherwise modified to obtain a variety of physical properties at a relatively low cost. For example, AE products with T_g of 0 °C or lower are used as pressure-sensitive adhesives. In addition, products with T_g of 0 °C or higher are used as paints and adhesives. Furthermore, T_g is strongly related to vibration damping properties, which is an essential parameter for its evaluation [20].

Therefore, this study investigates the relationship between the physical properties of water-based adhesives and the damping properties of wood-based materials. Master curves using the temperature–time conversion law were created from loss tangent of dynamic viscoelasticity (tanδ_D) obtained from the dynamic viscoelasticity of AE films with different T_gs and blends. In addition, tanδ_D was compared with flexural vibration property (tanδ_F) in lower and higher modes obtained from the flexural vibration tests of PBs made from the same AE.

Materials and methods

Materials

Table 1 summarizes the five types of AE used in the experiment and urea–formaldehyde adhesion (UF), and Table 2 presents these compounding ratios. The properties of AE were referred to the manufacturer's website [21, 22]. UF was evaluated as a comparative adhesive in the PB flexural vibration test. Ammonium sulfate [$(NH_4)_2SO_4$] 20% solution was used as a hardener of UF at 9.1%. The viscosity of UF was measured at 23 °C and 30/min using Brookfield viscometer (BMII viscometer, Toki sangyo, Tokyo, Japan).

The particles of PB are Japanese cypress (*Chamaecyparis obtusa*). The Japanese cypress chips were processed with a hammer mill (HM-3, Nara Machinery, Tokyo, Japan) and classified into a mesh size of 0.85–2.0 mm for 30 min using a sieve shaker (Analysette 3, Fritsch, Idar-Oberstein, Germany). The particles were dried absolutely in a heat air oven at 105 °C for $\geq$ 3 days.

Preparation of AE films

AE was cast into a polytetrafluoroethylene (PTFE) resin mold with a depth of 0.5–2 mm and formed a film at

Table 1 Property of adhesives

Adhesive name	Product name	Resin type	T_g (°C)	MFT (°C)	Viscosity (mPa·s, 23 °C)	Solid content (%)	Manufacturer
Ac-65	RIKABOND AP-96	Acrylic emulsion	− 65	0	3500	55.0	Japan coating resin
Ac-15	MOWINYL LDM7522		− 15	0	100–1000	50.4	
Ac13	MOWINYL DM774		13	23	3000–10000	46.2	
Ac41	MOWINYL 6520		41	50	200	45.8	
Ac90	RIKABOND ES-90		90	110	125–375	50.6	
UF	UB-S1	Urea–formaldehyde resin	–	–	900	60.0	J-CHEMICAL

Table 2 Adhesive name and composition

Adhesive name	Mixing ratio	
Ac-65/90	Ac-65:Ac90	1:1
Ac-65/13/90	Ac-65:Ac13:Ac90	1:1:1
UF	UB-S1:$(NH_4)_2SO_4$ 20wt% aq.	90.9:9.1

20 °C and 65% RH for ≥ 1 day. The Ac41 and Ac90, with a minimum film-forming temperature higher than room temperature $T_r = \sim 20$ °C, formed a film by oven-drying at 150 °C for 20–40 min by covering the PTFE resin mold with aluminum foil. The Ac90 after oven-dry with cracks on the surface was molded with a thickness of 0.2 mm by hot pressing for 10 s at 200 °C. The prepared films were cut to 30 mm × 6 mm with a cutter, which were dried using a vacuum dryer at 60 °C.

Dynamic viscoelastic measurements

The thermomechanical properties were determined using a dynamic thermomechanical analyzer (DMA 242 E, Netzsch, Selb, Germany). The AE films were analyzed from −80 to 150 °C at a ramp of 3 °C/min in tension mode with a span of 10 mm; amplitude of 10 μm; and frequency of 1, 5, 10, and 20 Hz.

Fabrication of PB

The particles put into a polyethylene bag with a capacity of 70 L were sprayed with AE using a spray gun. Distilled water was added to the highly viscous adhesives until they were sprayable. The spread rates were made to 9:1 for the oven-dry particles and AE nonvolatile content. The adhesive-coated particles were spread manually onto the press plate. Subsequently, the particles were pressed with a target board density of 0.8 g/cm^3, hot plate temperature of 180 °C, compression pressure of 2 MPa, compression time of 15 min, and a thickness of 10 mm. After 15 min of compression, the hot plate heater was turned off, and the pressure was maintained while cooling for ≤ 100 °C. In addition, eight specimens of 300 mm × 30 mm (length and width) were produced from PBs controlled at 20 °C and 65% RH for ≥ 2 weeks.

Flexural vibration test of PB

Figure 1 shows a diagram of the flexural vibration test with PB. The specimens were suspended by two threads at the positions of the diagram. The two threads were placed at the nodes position (ratio to length = 0.2242) of the first resonance mode of the specimens. A microphone (MI-1235, Ono sokki, Yokohama, Japan) with a preamplifier (MI-3111, Ono sokki, Yokohama, Japan) was installed at one end of the specimens. The vibrations were measured by hammering the end surface of the other end with a metal rod with such force that the specimens did not move from the top of the two threads. Almost no longitudinal vibration occurred during hammering the end surface at the specimen shape and thread positions. Moreover, obtaining flexural vibration with less noise in the resonance frequency of higher modes than the flat surface hammering was possible. The details are described later in this section. The measured values were Fourier-transformed using an FFT analyzer DS-3000 (DS-3000, Ono sokki, Yokohama, Japan). The dynamic Young's modulus (E_F) was calculated from Eq. (1) [23] using the first resonance frequency (f_1) of a power spectrum. The measurement environment was 20 °C and 65% RH. In the following equation, l is the specimen length, and ρ is the density:

$$E_F = \frac{4\pi^2 \cdot l^4 \cdot \rho \cdot f_1^2 \cdot A}{m_n^4 \cdot I} \quad (1)$$

Then, $\tan\delta_F$ of PB are calculated from Eq. (2) [24] using the resonance frequency of each mode (f_n) obtained from the power spectra and the slope of the vibration

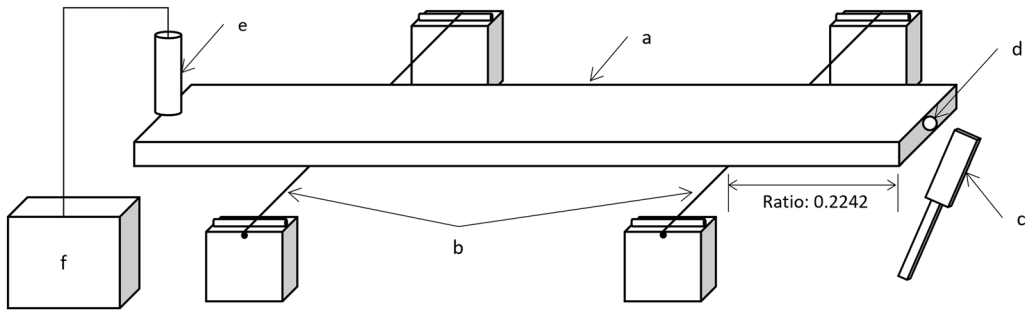

Fig. 1 Schematic of the flexural vibration test with PB; **a** PB specimen; **b** threads; **c** metal bar; **d** tapping point; **e** microphone with amplifier; and **f** FFT analyzer

damping (α) obtained from Hilbert transformed time base waveforms:

$$\tan\delta_F = 0.1151 \cdot |a| \cdot \frac{1}{\pi f_n} \quad (2)$$

Figure 2 shows the relationship between f_1–f_3 for different hammering positions on the end and flat surfaces in the vibration test. The specimens were a flat-grain board of solid Japanese cypress wood with grains in the longitudinal direction with the moisture content of 11.8% and PB made from UF. The dimensions of the solid wood were the same of PB. Therefore, almost no difference in f_1–f_3 was observed in both specimens. Furthermore, the f_1 of the present measurement was 200–600 Hz, whereas the f_1 of the longitudinal vibration using the 400–900-mm (length) specimens of keyaki (*Zelkova serrata*) in the previous report was approximately 5 kHz, confirming that the present results were due to flexural vibration [25].

Results and discussion

Dynamic viscoelasticity of AE films

Figure 3 shows the storage elastic modulus (E'), loss of elastic modulus (E''), and $\tan\delta_D$ of AE and blended AE at the measurement frequency of 10 Hz. The E'' of single AE peaked at a temperature slightly higher than T_g presented by the manufacturer. The E'' of single AE peaked at a temperature slightly higher than T_g presented by the manufacturer, and E' showed a glassy state up to around that temperature; it also dropped sharply as increased temperature. The $\tan\delta_D$ of single AE showed a clear peak according to each T_g. This suggests that the molecular structure is in the form of homopolymers or random copolymers [26]. However, E' and E'' of blended Ac-65/90 decreased more gradually than AE single from −60 to 120 °C and decreased significantly with a different slope after 120 °C. The $\tan\delta_D$ of Ac-65/90 showed peaks at ~ −30 °C and 120 °C similar to single Ac-65 and Ac90, showing flat behavior between them. This phenomenon, in which separate peaks appeared, suggests that the two AEs may be phase-separated in the film [27]. The E' and E'' of blended Ac-65/13/90 showed the same tendency as those of Ac-65/90. Besides, the E' peak based on T_g of Ac13 was confirmed after 50 °C. However, the $\tan\delta_D$ of Ac-65/13/90 showed almost no peak at ~ −30 °C derived from Ac-65, showing a higher value for the peak on the higher temperature side. It indicates that Ac90 forms a continuous layer during the film formation [27].

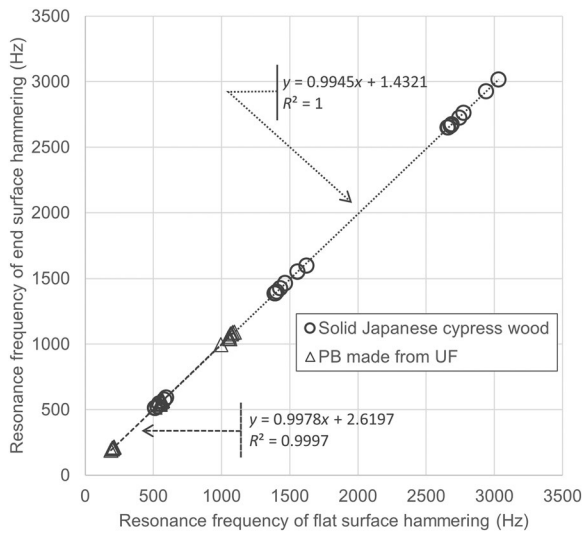

Fig. 2 Relationship between f_1–f_3 for different hammering positions on the end and flat surfaces in the vibration test

Analysis of $\tan\delta_D$ due to master curve

To study the frequency characteristics of $\tan\delta_D$ in a wider range, the master curves were prepared at the reference temperature of $T_0 = 20$ °C and the measured temperature of $T = -20$ °C to 50 °C using the time–temperature conversion rule [28]. T_0 is presumed to be the room temperature in Japan. During the preparation, it was arranged around T_0 so that the results on the low- and high-temperature sides were translated to the high- and low-frequency sides, respectively, to form a single curve. Figure 4 shows the details of the master curve creation.

Figure 5 shows the master curves of $\tan\delta_D$ at T_0 in the scope of 1–10,000 Hz. The solid lines in the master curve are the result of visually connecting the rough trend of the plot. The $\tan\delta_D$ of Ac-65 with the lowest T_g showed a leveling off to ~1–400 Hz. However, there were some variations; a gradual upward trend was observed as the frequency increased. We presumed that this variation is due to the difficulty of measuring rubber-state samples from T_r to high-temperature ranges in tensile mode. The $\tan\delta_D$ of Ac-15 was the largest value among the specimens and peaked at ~50 Hz. The measured temperature of ~7 °C on the viscoelasticity corresponds to one digit of the reduced frequency on a master curve [17]. In this study, a similar tendency was shown in the master curve because the $\tan\delta_D$ peak measured at 10 Hz of Ac-15 in Fig. 3 is 16 °C. The $\tan\delta_D$ of Ac13, Ac41, and Ac90 was lower than that of the aforementioned two types at any reduced frequency. Because the three types of AE have T_g greater than or equal to T_0, it is considered that the master curves strongly reflected the results of the glassy state. The $\tan\delta_D$ of blended Ac-65/90 showed an intermediate value between Ac-65 and Ac90. However, the value shifted to the Ac90 side as the reduced frequency increased. It is possible that the phase-separated

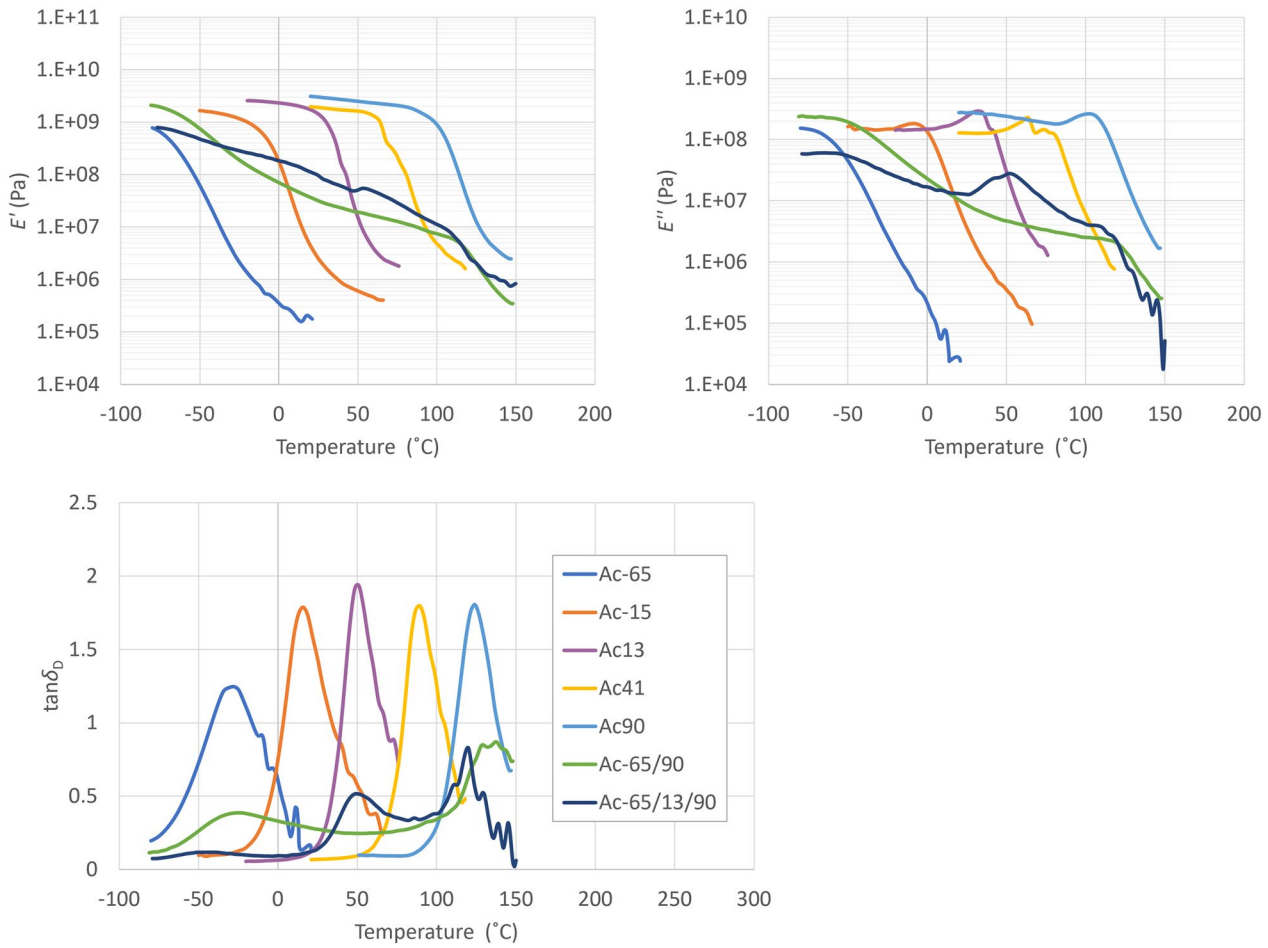

Fig. 3 Dynamic viscoelastic properties of AE and blended AE films

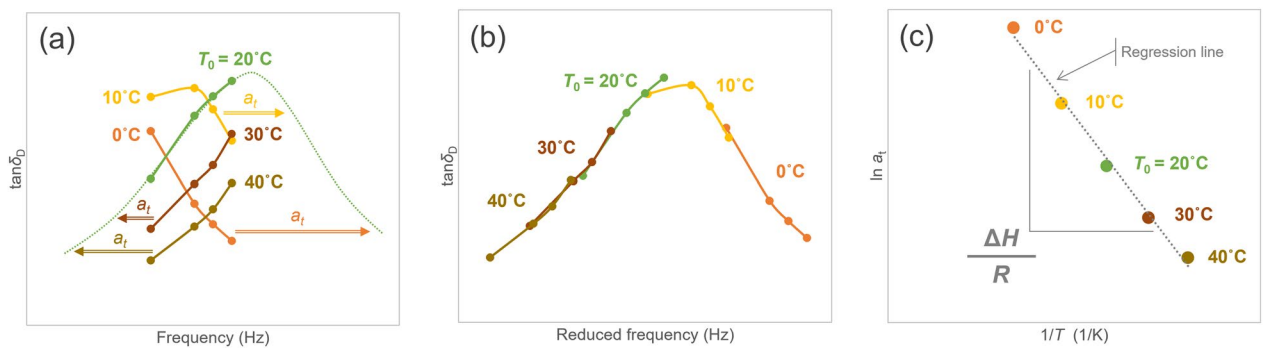

Fig. 4 Details of the master curve creation; **a** the value of low temperature is shifted to the high frequency side and the value of high temperature is shifted to the low-frequency side based on T_0 so that they overlap on the single line; **b** the master curve overlapped on the single line; **c** calculate ΔH by finding the slope of the tangent line from an Arrhenius-type plot with the reciprocal of the absolute temperature on the horizontal axis and natural logarithm of a_t on the vertical axis

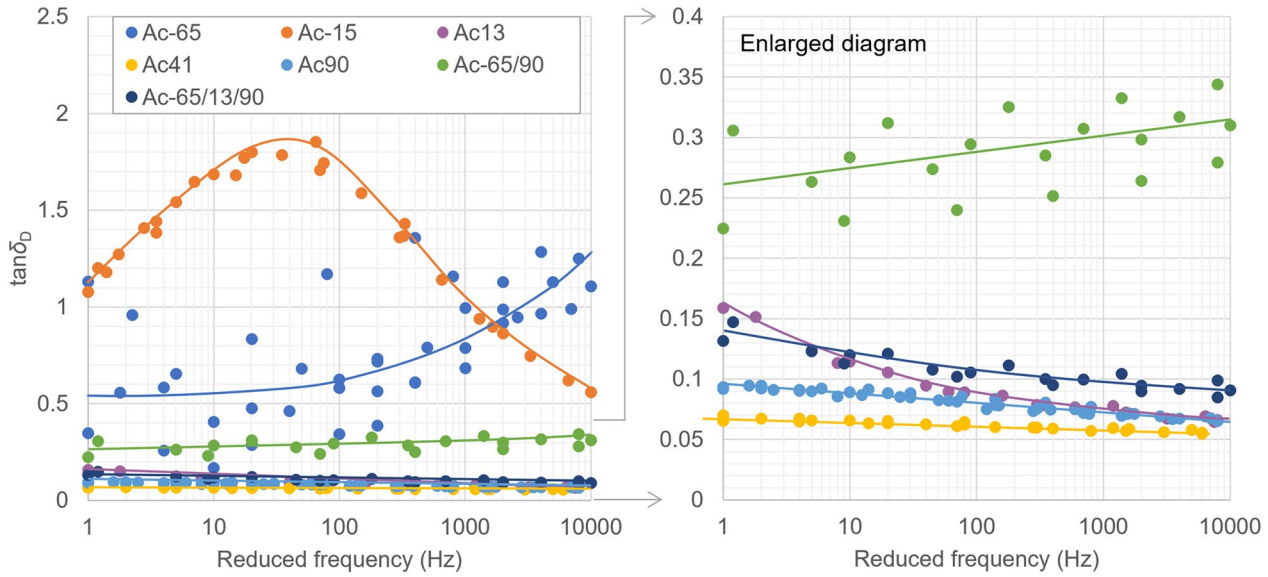

Fig. 5 Master curve of $\tan\delta_D$ at T_0; reference temperature 20 °C; measured temperature — 20 to 50 °C

adhesive formed a sea–island structure with Ac90 and Ac-65 on the sea and island sides, respectively, making it more susceptible to Ac90. The $\tan\delta_D$ of Ac-65/13/90 was lower than that of Ac-65/90. The reason is that the addition of Ac13 increased the proportion of glassy components in T_0.

The shift factor (a_t), which is the amount of parallel translation at the placement time, was expressed by the Arrhenius equation using Eq. (3) [29]. Therefore, the apparent activation energy ΔH in viscous flow was calculated from the slope of the tangent by plotting $\ln a_t$ at $1/T$. R is the gas constant:

$$\ln a_t = \frac{\Delta H}{R} \cdot \left(\frac{1}{T} - \frac{1}{T_0} \right) \tag{3}$$

Figure 6 shows the relationship between $\ln a_t$ of each AE and $1/T$. Table 3 presents ΔH in the viscous flow of each AE. First, in all AEs, the high correlation with a coefficient of determination $R^2 \geq 0.95$ was observed using linear approximation, confirming the validity of the master curve. The ΔH of single AE achieved a maximum value at Ac13 and decreased with the change of temperature. This is owing to the fact that ΔH depends on the scale of molecular motion, and the micro-Brownian motion, called the main dispersion, shows an extreme near T_g [26]. Therefore, ΔH becomes progressively smaller as the T_g of AE moves away from T_0. The ΔH of Ac-65 and Ac90 are considered to have shown almost the same value because T_g was far away from T_0 and T. The ΔH of blended AE differs depending on its T_g. Ac-65/90 blended with only AE with low ΔH and was almost the same as the two AEs before blending. However, Ac-65/13/90 shows similar results to Ac13, suggesting that AE with a high ΔH may have a strong effect on ΔH even after blending. In addition, Ac13 and Ac-65/13/90 can be seen as if the slope of $\ln a_t$ changed at ~ 10 °C (Fig. 7). This temperature is close to T_g of Ac13; the fluidity of both AEs likely changed at the boundary of T_g [29]. In addition, Ac-15 and Ac41, whose T_g is in the range of T, are assumed to have the same trend. However, no clear trend was observed, probably due to the fact that the T_gs deviated significantly from T_0.

Flexural vibration of PB

Figure 8 shows E_F and ρ in the flexural vibration test of PB prepared with various AEs and UF. E_F of single AE was maximum at Ac13 and declined as T_g of AE increased and decreased. The reason is that the shear bonding strength of AE could influence E_F [30]. The Young's moduli in the flexure of PB are proportional to the shear bonding strengths of adhesives [31]. In addition, shear bonding strengths of thermoplastic adhesives have a maximum value at T_r when T_g is the T_r [32]. E_F of blended AE showed a similar tendency to that of Ac41 and Ac90. It had a value slightly higher than the average value calculated from the compounding ratios of AE (Table 4). We presumed that this result is because the phase structure of blended AE is susceptible to AE with high T_g (Fig. 7). UF's E_F is also equivalent to Ac90.

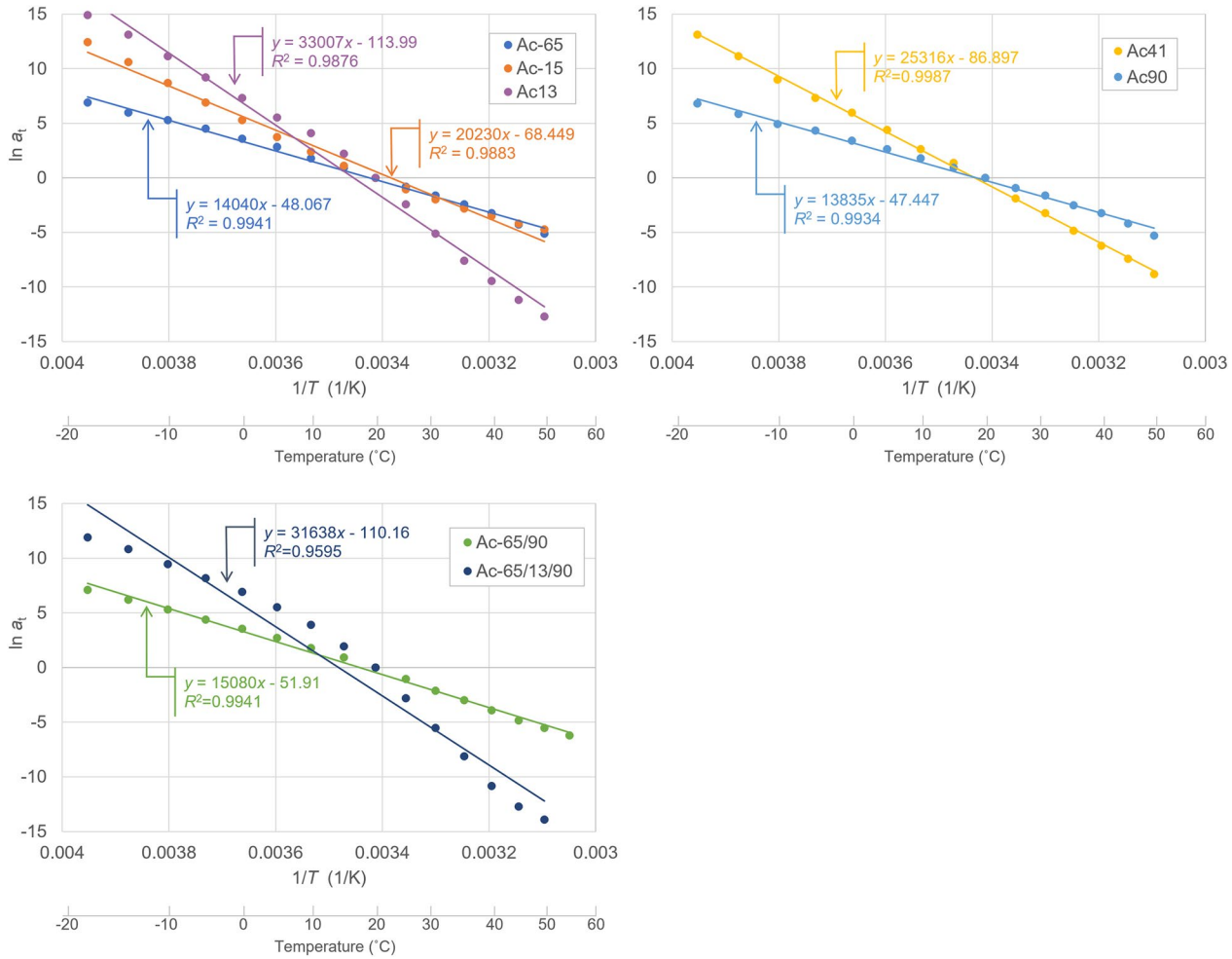

Fig. 6 Temperature dependence of the shift factor ln a_t in AE and blended AE films; to match the display of Celsius temperature, 1/T is shown inverted

Table 3 ΔH in master curves of various AEs

Adhesive name	ΔH (kJ/mol)
Ac-65	116.7
Ac-15	168.2
Ac13	274.4
Ac41	210.5
Ac90	115.0
Ac-65/90	125.4
Ac-65/13/90	263.0

Figure 9 shows the relationship between f_n and tanδ_F of PB prepared with various AEs and UF. Table 5 shows the average value and standard deviation (SD) of f_n and tanδ_F. The tanδ_F of Ac-65 and Ac-15 values are higher than other AEs. In addition, Ac-15 showed a decreasing

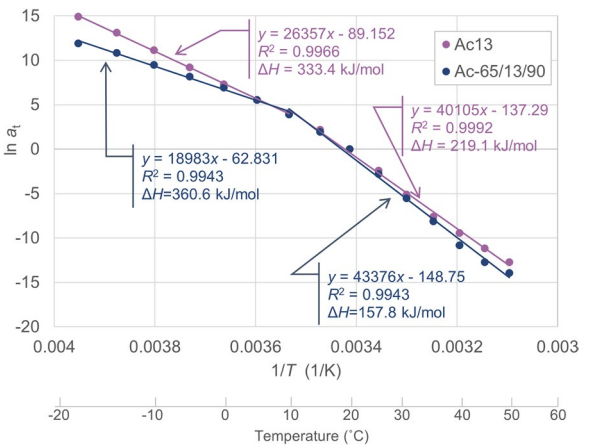

Fig. 7 Temperature dependence of the shift factor ln a_t in AE, including Ac13; to match the display of Celsius temperature, 1/T is shown inverted

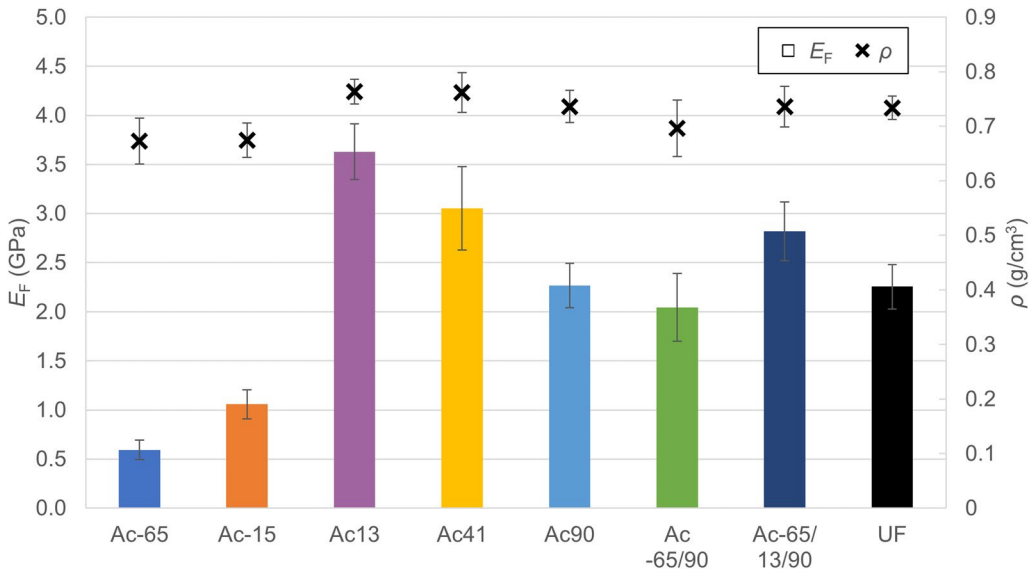

Fig. 8 E_F and ρ in the flexural vibration test of PB; the error bars indicate standard deviation

Table 4 Measured value of blended AE and averaged value calculated from an AE simple substance in E_F of particle board

Adhesive name	Calculated ratio	E_F (MPa)
Ac-65/90		
Measured value	–	4958
Averaged value	1:1	3648
Ac-65/13/90		
Measured value	–	6761
Averaged value	1:1:1	5347

tendency with an increase in f_n. The reason is that the two AEs in the glass transition or rubber regions at $T = 20$ °C easily absorb vibration (Fig. 3). All other AEs showed small values since they were in the glassy or glass transition regions near it. When the vertical axis was expanded, Ac13 showed a gradual decreasing tendency and Ac-65/90 showed a gradual increasing tendency. The tendencies of other AEs and UF were broadly flat, although there were some variations.

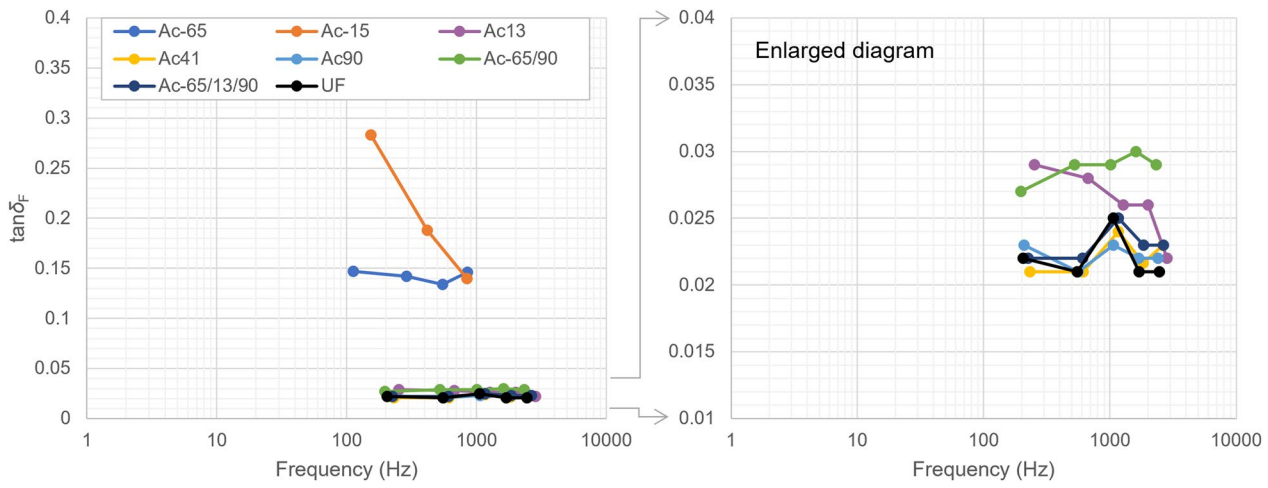

Fig. 9 Relationships between frequency and tanδ_F in the flexural vibration test of PB

Table 5 Average value and SD of f_n and tanδ_F for various AEs

Adhesive name	Avg./SD	Resonance frequency (Hz)					tanδ_F				
		f1	*f2*	*f3*	*f4*	*f5*	*f1*	*f2*	*f3*	*f4*	*f5*
Ac-65	Avg.	112.3	289.8	550.2	849.6	–	0.147	0.142	0.134	0.146	–
	SD	7.5	21.5	49.3	73.1	–	0.0463	0.0384	0.0306	0.0147	–
Ac-15	Avg.	153.5	417.5	842.1	–	–	0.283	0.188	0.140	–	–
	SD	8.1	16.2	34.3	–	–	0.0775	0.0471	0.0158	–	–
Ac13	Avg.	252.3	673.1	1272.3	2002.3	2836.5	0.029	0.028	0.026	0.026	0.022
	SD	5.0	9.0	16.4	22.9	37.3	0.0011	0.0011	0.0032	0.0011	0.0019
Ac41	Avg.	232.1	615.0	1162.2	1836.9	2620.8	0.021	0.021	0.024	0.022	0.023
	SD	11.0	24.6	49.7	69.7	97.0	0.0006	0.0006	0.0041	0.0008	0.0026
Ac90	Avg.	209.2	558.8	1062.1	1684.4	2406.0	0.023	0.021	0.023	0.022	0.022
	SD	7.3	20.4	40.6	63.1	84.1	0.0011	0.0014	0.0023	0.0017	0.0013
Ac-65/90	Avg.	197.5	524.4	1009.4	1608.8	2324.4	0.027	0.029	0.029	0.030	0.029
	SD	11.7	33.8	66.8	100.8	151.3	0.0009	0.0006	0.0038	0.0035	0.0017
Ac-65/13/90	Avg.	225.6	610.0	1165.0	1848.8	2640.7	0.022	0.022	0.025	0.023	0.023
	SD	6.8	20.8	38.5	61.5	94.2	0.0003	0.0003	0.0024	0.0006	0.0017
UF	Avg.	205.6	551.9	1059.6	1695.6	2455.3	0.022	0.021	0.025	0.021	0.021
	SD	8.1	15.6	29.9	44.5	60.0	0.0005	0.0003	0.0018	0.0003	0.0006

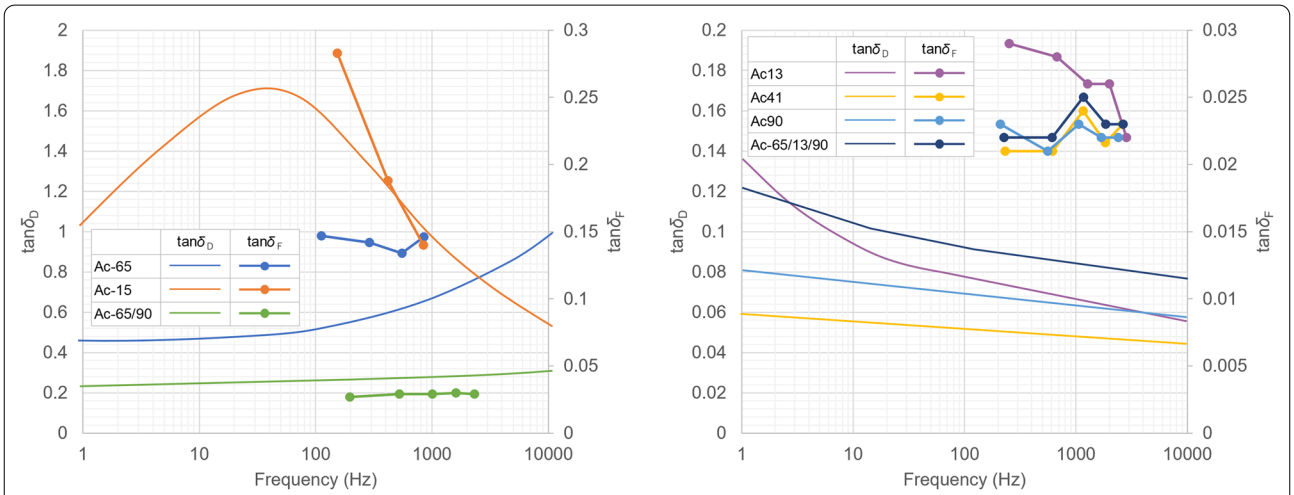

Fig. 10 Relationships between frequency, tanδ_D, and tanδ_F in various AEs

Comparison of tanδ_D and tanδ_F

Figure 10 shows the comparison results of tanδ_D and tanδ_F in the frequency of 1–10,000 Hz. The magnitudes of the two tanδs differed by ~3–10 times; however, they have the same tendencies. We presumed that this is because the relationship between the adhesive and particles in PB is similar to the sea–island structure. It was strongly influenced by adhesives as the sea side. Furthermore, regarding frequency dependence, similar tendencies were observed for all AEs, except for Ac-65. Generally, Ac-65 should show a similar tendency. However, there were variations during tapping since it was in a rubber state at this measurement temperature.

Conclusions

In this study, we evaluated tanδ_D of films made from AEs with different T_g and tanδ_F of PB to investigate the relationship between the physical properties of water-based adhesives and the vibration damping properties of wood-based materials. We obtained the following conclusions:

1. The peaks of E', E'', and $\tan\delta_D$ with a single AE obtained from $\tan\delta_D$ were confirmed according to each T_g. E' and E'' of blended AE decreased gradually from −60 to 120 °C; more than 120 °C changed its slope. $\tan\delta_D$ of blended AE was confirmed as the peak-based phase separation; its peak was smaller than AE alone.
2. $\tan\delta_D$ of the master curve at a frequency of 1–10,000 Hz showed a high value at T_0 for Ac-65 in the rubber state and Ac-15 in the glass transition state. However, it showed a low value for the other AEs for the glassy state. ΔH calculated from ln a_t showed high values for Ac13 and Ac-65/13/90.
3. E_F of single AE in the flexural vibration test showed the maximum value at Ac13 and declined as T_g of AE increased and decreased. The E_F values of blended AE and UF were similar to Ac41 and Ac90. The $\tan\delta_F$ values were high in Ac-65 in the rubber state and Ac-15 in the transition state; it was low in other cases.
4. According to these results, $\tan\delta_D$ and $\tan\delta_F$ showed a similar tendency in most AEs in terms of frequency dependence.

Abbreviations

PB: Particle board; AE: Acrylic emulsion adhesive; T_g: Glass transition; $\tan\delta_D$: Loss tangent of dynamic viscoelasticity; $\tan\delta_F$: Loss tangent of flexural vibration property; ΔH: Apparent activation energy; E_F: Dynamic Young's modulus; UF: Urea–formaldehyde adhesion; RC: Reinforced concrete; SRC: Steel-framed reinforced concrete; CLT: Cross-laminated timber; $\tan\delta$: Loss tangent; PTFE: Polytetrafluoroethylene; T_r: Room temperature; f_1: First resonance frequency; l: Specimen length; ρ: Density; f_n: Resonance frequency of each mode; α: Slope of vibration damping; E': Storage elastic modulus; E'': Loss of elastic modulus; T_0: Reference temperature; T: Measured temperature; a_t: Shift factor; R: Gas constant; R^2: Coefficient of determination; SD: Standard deviation.

Acknowledgements

The authors would like to thank Mitsubishi Chemical Corporation and J-CHEMICAL Inc. for providing the adhesives. We also thank the Industrial Research Institute of Shizuoka Prefecture for lending us the equipment.

Authors' contributions

KF and MY have participated sufficiently in the work to take public responsibility for the entire content of the manuscript. TI, HS, and RM have participated sufficiently in the work to take public responsibility for part of the content of the manuscript. All authors read and approved the final manuscript.

Funding

This work was supported by JSPS KAKENHI Grant Number 18K05759.

Availability of data and materials

Not applicable.

Declarations

Ethics approval and consent to participate

Not applicable.

Consent for publication

Not applicable.

Competing interests

The authors declare that they have no competing interests.

Author details

[1]The United Graduate School of Agricultural Science, Gifu University, 1-1 Yanagido, Gifu 501-1193, Japan. [2]Graduate School of Integrated Science and Technology, Department of Agriculture, Shizuoka University, 836, Ohya, Suruga-ku, Shizuoka 422-8529, Japan. [3]Faculty of Agriculture, Shizuoka University, 836, Ohya, Suruga-ku, Shizuoka 422-8529, Japan.

Received: 1 October 2021 Accepted: 4 February 2022
Published online: 12 March 2022

References

1. United Nations (2018) World urbanization prospects 2018 highlights. Department of Economic and Social Affairs, Population Division, New York, USA; pp 5–7
2. Maschke C, Niemann H (2007) Health effects of annoyance induced by neighbour noise. Noise Control Eng 55(3):348–356
3. Lee PJ, Kim YH, Jeon JY, Song KD (2007) Effects of apartment building façade and balcony design on the reduction of exterior noise. Build Environ 42(10):3517–3528
4. Ministry of Internal Affairs and Communications (2018) Pollution complaint survey in 2017. Tokyo, Japan, p 9 (**in Japanese**)
5. Minemura A, Ishikawa Y (2000) Study for reduction of the floor impact sound level by using of the damping materials: part 5: study of the vibration response characteristics of the concrete slab. AIJ J Technol 10(6):139–142 (**in Japanese**)
6. Sueyoshi S, Yamamoto K, Kobayashi M, Yamaguchi M (2003) Psychoacoustical evaluation of floor impact sounds from a concrete slab with damping materials attached: study for reduction of the floor impact sound level by using of the damping materials: part 6. AIJ J Technol 17(6):229–232 (**in Japanese**)
7. Sakamoto K, Inoue K, Akimoto K (2017) A study on the heavy floor impact sound insulation performance in a wooden long-span structure building: an experimental study on improvement methods of floor impact sound insulation performance with floor structure specification part 1. J Environ Eng AIJ 82(736):535–542 (**in Japanese**)
8. Tanaka M, Murakami T, Kasai Y, Kawai M (2017) Floor impact sound insulation performance of CLT floor slab and reduction effect by floor coverings. AIJ J Technol 23(55):903–908 (**in Japanese**)
9. Tanaka M, Murakami T, Kasai Y (2017) Study on floor impact sound reduction effect by double ceiling system with cross laminated timber panels. J Environ Eng AIJ 82(736):543–550 (**in Japanese**)
10. Architectural Institute of Japan (2016) Guidance for evaluation and design of sound insulation in apartment houses. Archi Books, Tokyo, pp 34–35 (**in Japanese**)
11. Wang Z, Li L, Gong M (2012) Measurement of dynamic modulus of elasticity and damping ratio of wood-based composites using the cantilever beam vibration technique. Constr Build Mater 28(1):831–834
12. Guan C, Zhang H, Hunt JF, Yan H (2016) Determining shear modulus of thin wood composite materials using a cantilever beam vibration method. Constr Build Mater 121:285–289
13. Ebihara T (2001) Development of vibration absorbable woody board. Res J Food Agric 24(11):9–13 (**in Japanese**)
14. Lee HJ, Hatano Y, Mizumachi H, Hotta Y, Fukui T (1994) Damping properties of wood/polymer composites I: comparison of longitudinal vibration and flexural vibration of laminates. Mokuzai Gakkaishi 40(10):1027–1035 (**in Japanese**)
15. Lee HJ, Mizumachi H (1994) Damping properties of wood/polymer composites II: influence of viscoelastic properties of polymer layer on flexural vibration of laminates. Mokuzai Gakkaishi 40(10):1036–1043 (**in Japanese**)

16. Lee HJ, Mizumachi H (1994) Damping properties of wood/polymer composites III: influence of geometry on flexural vibration of laminates. Mokuzai Gakkaishi 40(10):1044–1051 (**in Japanese**)
17. Lee HJ, Mizumachi H (1995) Damping properties of wood/polymer composites IV: 2-ethylhexylacrylate/styrene copolymer and interpenetrating polymer networks. Mokuzai Gakkaishi 41(1):9–16 (**in Japanese**)
18. Lee HJ, Mizumachi H (1994) Damping properties of wood/polymer composites: preparation of epoxide resin blends and IPNs showing a broad damping peak. J Adhesion Soc Jpn 30(7):313–320 (**in Japanese**)
19. Sargianis JJ, Kim HI, Andres E, Suhr J (2013) Sound and vibration damping characteristics in natural material based sandwich composites. Compos Struct 96:538–544
20. Ogawa T (2008) Adhesives with vibration damping properties. J Adhesion Soc Jpn 30(7):313–320 (**in Japanese**)
21. Japan Coating Resin Corporation (2021) Products, Paint binder(s). https://www.jc-resin.com/english/product/toryo.html. Accessed 8 Jan 2022
22. Japan Coating Resin Corporation (2021) Products, pressure sensitive adhesives. https://www.jc-resin.com/english/product/nenchaku.html. Accessed 8 Jan 2022
23. Kubojima Y, Tonosaki M, Yoshihara H (2005) Effect of additional mass on the Young's modulus of a wooden beam. J Test Eval 33(4):278–282
24. Ono Sokki Corp (2015) Portable FFT analyzer model CF-7200: damping factor measurement to use the Hilbert transform. Ono Sokki Corp, p 6. https://www.onosokki.co.jp/English/hp_e/c_support/ope_manual/pdf/cf7200_hilbert.pdf. Accessed 11 Jun 2021
25. Sobue N (1986) Measurement of Young's modulus by the transient longitudinal vibration of wooden beams using a fast Fourier transformation spectrum analyzer. Mokuzai Gakkaishi 32(9):744–747
26. Takahara A (2009) Dynamic viscoelastic properties-from bulk to surface of polymeric solids. Sen'i Gakkaishi 65(12):472–476 (**in Japanese**)
27. Suzuki K, Kitamura T (2005) Study on film properties composed of blended acrylic latexes. Toryono kenkyu 144(10):9–16 (**in Japanese**). https://www.kansai.co.jp/rd/token/pdf/144/03.pdf. Accessed 11 Jun 2021
28. Ferry JD (1980) Viscoelastic properties of polymers, 3rd edn. Wiley, New York, pp 264–270
29. Hamada H, Tsunosawa H (1997) Correlation between internal structure and time-temperature dependence on bending properties of PC/ABS blend injection moldings. J Soc Mat Sci Jpn 46(1):89–95 (**in Japanese**)
30. Fujishiro K, Nagaya H, Ito T, Yamada M, Maeda K, Nagasawa T (2019) Wood bonding performance and vibrational properties of acrylic resin blend emulsion with different glass transition. In: proceeding of the 57th symposium of the Adhesion Society of Japan, Kitakyushu, 19–20 Jun 2019, pp 81–82 (**in Japanese**)
31. Çetin NS, Özmen N (2002) Use of organosolv lignin in phenol-formaldehyde resins for particleboard production II. Particleboard production and properties. Int J Adhes Adhes 22(6):481–486
32. Mizumachi H (1981) Influence of the physical properties of adhesive polymers upon wood adhesion. Wood Ind 36(2):57–61 (**in Japanese**)

Publisher's Note